A novel hybrid model for the motion of sustained axisymmetric gravity currents and intrusions

M. Ungarish [a], C.G. Johnson [b,*], A.J. Hogg [b]

[a] *Department of Computer Science, Technion, Haifa 32000, Israel*
[b] *Centre for Environmental & Geophysical Flows, School of Mathematics, University of Bristol, UK*

ARTICLE INFO

ABSTRACT

We consider the sustained propagation of axisymmetric intrusions and gravity currents through linearly stratified or unstratified ambient fluids. Such flow configurations are found in a number of atmospheric and oceanic flows, in particular the predominantly horizontal spreading of a volcanic ash cloud after it has ascended through the atmosphere. There is strong theoretical evidence that these flows consist of two domains: an outer annular 'head' at the front of the current in which the motion is unsteady; and an inner, much thinner 'tail', which is steady, but spatially varying. The transition between the regions is a moving hydraulic jump. While it is possible to investigate these motions by numerically integrating the governing shallow layer equations, here we develop a much simpler mathematical model, which reproduces the more complicated model accurately and addresses issues such as what determines the position of the front and the moving bore between the two regions; what is the partition of influxed volume between the tail and head; and what is the distribution of suspended particles in the flow if present at the source? In such settings a conventional integral model fails, as does scaling based on dimensional analysis and the anticipation of an underlying self-similar form; the predictions they yield for these flows are incorrect. Instead we present a new hybrid model, which combines exact results of the steady shallow-water equations in the tail with simplifying assumptions in the head. This model predicts the flow properties by the straightforward solution of three ordinary differential equations (for front and bore positions and the volume fraction of particles in the head), without using adjustable constants, and obtains the correct asymptotic behaviour for the radius of the current r_N with respect to time t, namely $r_N \sim t^{4/5}$ for gravity currents and $r_N \sim t^{3/4}$ for intrusions. The predictions are obtained with negligible computational effort and accurately capture results from the more complete shallow water models. The model is also applied with success to gravity currents and intrusions that carry particles. For flows in which it is the presence of the particles alone that drives the motion, we identify length and time scales for the runout in terms of dimensional parameters that characterise the release, thus establishing the hybrid model as a useful tool also for modelling radial runout.

1. Introduction

In this contribution we study the sustained propagation (from a constant source) of axisymmetric intrusions and gravity currents at high Reynolds number. More specifically, we study the motion of a sustained volume flux of fluid flowing from a point source into a quiescent ambient, which is either unstratified or linearly stratified. If the ambient is stratified, this influx may form an intrusion about its level of neutral buoyancy (the height at which the density of the environment matches the density of influx). If instead the inflow is denser (or less dense) than any part of the ambient, there is no neutral buoyancy level, and the influx will flow as a gravity current over the horizontal base (or uppermost surface) of the ambient. Sustained, axisymmetric buoyancy-driven flows in both these regimes are observed in a range of environmental flows, including river outfalls [1], intrusions into stratified lakes [2] and volcanic plumes [3,4].

The buoyancy-driven spreading of intrusions is of particular practical importance due to the transport of volcanic ash by such flows. A volcanic plume rises from the vent until it reaches a height at which its density matches that of the atmosphere, whereupon it

* Corresponding author. Tel.: +44 7792640138.
E-mail addresses: unga@cs.technion.ac.il (M. Ungarish), chris.johnson@bristol.ac.uk (C.G. Johnson), a.j.hogg@bristol.ac.uk (A.J. Hogg).
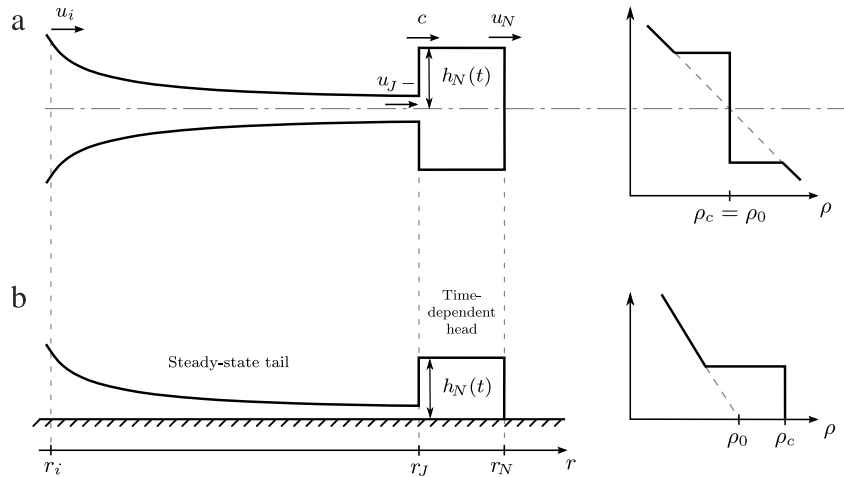
Fig. 1. Sketch of the radial height profile (left) and vertical density profile (right) of an intrusion (a), and a gravity current (b). In an intrusion, the buoyancy frequency, which measures the ambient density gradient, satisfies $\mathcal{N}^2 > 0$, the density of the current $\rho_c = \rho_0$ and $h(r, t)$ represents the half-height of the flow. In a gravity current, $\mathcal{N}^2 \geq 0$, $\rho_c \neq \rho_0$ (here, for currents denser than the ambient, $\rho_c > \rho_0$) and h represents the full height of the flow. Then for hybrid models, we assume that within the frontal region – the annulus between a hydraulic jump at $r = r_J(t)$ and the flow front at $r = r_N(t)$ – the flow height is spatially constant and equal to $h_N(t)$.

begins to spread horizontally. Importantly, the volumetric concentration of ash is sufficiently small so that it contributes only negligibly to the density of the volcanic cloud (see, for example, the typical volume fraction of particles at the top of the plume computed by Woodhouse et al. [5]). The intrusion spreads horizontally, therefore, because it has perturbed the background stratification, generating a well-mixed flowing layer (see Fig. 1). In the absence of wind, or if the wind speed is much less than the spreading rate of the intrusion, the ash cloud spreads radially, potentially transporting ash particles over considerable distances [4]. The challenge of predicting the dynamics of these clouds is important due to the significant hazard to aircraft flight that volcanic ash poses [6].

While the examples given so far have featured flows in which the density of the flowing layer remains constant, 'particle-driven' flows often arise in environmental settings, such as oceanic turbidity currents (see, for example [7–9], and references therein). In these flows, the presence of relatively heavy suspended particles contributes significantly to the overall density. These particles progressively sediment out of the flow, diminishing the density difference between the current and the ambient and reducing the driving force. Quantitative models of such flows necessarily couple the evolution of the suspension to the height and velocity of the flowing layer [7].

1.1. Shallow-layer models

One approach to modelling both gravity currents and intrusions exploits the thinness of the flows relative to their radial extent. In such thin flows, the excess pressure is hydrostatic to leading order and the flow is predominantly horizontal [10–12]. Both intrusions and gravity currents can be modelled within the same framework by including both the difference in density between the current and ambient and gradients of the ambient fluid density [12,13], and we present the equations in this form before considering the two types of flow separately. We denote the density of the intrusion or gravity current by ρ_c and the gradient of the ambient fluid density by $-\mathcal{N}^2 \rho_c / g$, where $\mathcal{N}$ is the constant buoyancy frequency of the stably stratified ambient fluid. The reference density ρ_0 is the density of the ambient at the horizontal plane of symmetry of an intrusion, or at the base of a gravity current (Fig. 1). For a gravity current, $\rho_c > \rho_0$, and either $\mathcal{N} = 0$ (a uniform ambient) or $\mathcal{N} > 0$ (a stably stratified ambient). For an intrusion into a stratified ambient fluid centred about its neutral buoyancy height, $\rho_c = \rho_0$ and $\mathcal{N} > 0$. We note that although the density of

an intrusion is the same as the average density of the fluid it displaces, it may nevertheless be thought of as a buoyancy-driven flow because the thickness of the intrusion, over which the density is uniform, means that there are density differences between the intruding fluid and the ambient.

The layer-averaged radial velocity of the flow is denoted as u and the flow thickness h, both functions of the radial coordinate, r, and time, t. While for a gravity current, h denotes the full thickness of the current, for an intrusion h denotes the half-thickness, and is measured from the neutral-buoyancy level to the upper interface; the lower interface is the mirror image (see Fig. 1).

Shallow-layer equations expressing the conservation of mass and balance of momentum have been developed to model the evolution of u and h, and are given by (see, for example [12,14, sections 13 and 16.3]),

$$\frac{\partial h}{\partial t} + \frac{1}{r}\frac{\partial}{\partial r}(rhu) = 0 \tag{1}$$

and

$$\frac{\partial}{\partial t}(uh) + \frac{1}{r}\frac{\partial}{\partial r}(ru^2h) + \frac{\partial}{\partial r}\left(\frac{1}{2}g'h^2 + \frac{1}{3}\mathcal{N}^2h^3\right) = 0 \tag{2}$$

where g' is the reduced gravity $(\rho_c - \rho_0)g/\rho_0$. Conservation of mass (1) is derived on the neglect of mixing with the surrounding fluid, while the momentum balance (2) is derived under the assumptions that drag is negligible, and that density differences are sufficiently small so that the flow is Boussinesq.

Gravity currents and intrusions may transport relatively dense particles in suspension, which settle with velocity w_s. Denoting the volume fraction of particulate by ϕ, a shallow layer model for its evolution is given by

$$\frac{\partial \phi}{\partial t} + u\frac{\partial \phi}{\partial r} = -\frac{w_s\phi}{d}, \tag{3}$$

where d denotes the total depth of the flowing layer; for gravity currents $d = h$, while for intrusions $d = 2h$. In this model it has been assumed that the flow is sufficiently turbulent to maintain a well-mixed suspension and that the suspension is sufficiently dilute that particle–particle interactions are prevented (see, for example [7]). The bulk density of the current is given by

$$\rho_c = \rho_f + (\rho_p - \rho_f)\phi, \tag{4}$$

where ρ_f and ρ_p are respectively the densities of the interstitial fluid and suspended particles. If $(\rho_p - \rho_f)\phi \ll |\rho_0 - \rho_f| + \rho_0$

$\mathcal{N}^2 h/g$ then the particles are dynamically passive; they are merely advected by the flow and settle out of suspension. We term these flows 'particle-laden' and will examine their dynamics in the context of ash-laden intrusions (see Section 4.1). However, if $(\rho_p - \rho_i)\phi = O(|\rho_0 - \rho_i| + \rho_0 \mathcal{N}^2 h/g)$, the particles contribute significantly to the bulk density of the current and this couples the governing equations. We term these flows 'particle-driven' and examine in Section 4.2 the dynamics of gravity currents propagating through uniform environments when the excess density of the current is due only to the presence of suspended particles ($\rho_i = \rho_0$).

The three Eqs. (1)–(3) form a hyperbolic system in which the three characteristic speeds, which we denote by c_+, c_- and c_p, are $c_\pm = u \pm (\mathcal{N}^2 h^2 + g'h)^{1/2}$ and $c_p = u$. The governing equations are subject to initial and boundary conditions. While the source is active, the intrusion extends from a fixed inlet radius r_i to the moving front at radius $r_N(t) > r_i$. At the inlet radius $r = r_i$, we specify the volume flux of fluid per unit radian, q, in the gravity current or in the upper half of the intrusion and the volume fraction of particles (if present)

$$ruh = q \quad \text{and} \quad \phi = \phi_0 \quad \text{at } r = r_i. \tag{5}$$

The total volume flux of the gravity current is therefore $2\pi q$ and the volume flux of the intrusion is $4\pi q$. Additionally, if the flow is supercritical (by which we mean that there is no upstream propagation of perturbations, from the main body of intrusion to the inlet i.e., $c_- \geq 0$), then we also specify the source energy density per unit mass, $E/2$, as

$$u^2 + 2g'h + \mathcal{N}^2 h^2 = E \quad \text{at } r = r_i. \tag{6}$$

This may be thought of as the Bernoulli constant for an inviscid flow within a linearly stratified environment. Alternatively we could have specified an inlet Froude number $Fr_i = u_i/(\mathcal{N}^2 h_i^2 + g'h_i)^{1/2}$, in which case E can be represented implicitly as a function of Fr_i, $\mathcal{N}$, g' and r_i. In an intrusion, $g' = 0$ and the relationship is explicit,

$$E = \frac{\mathcal{N}q}{r_i Fr_i}\left(1 + Fr_i^2\right). \tag{7}$$

Likewise, in a gravity current propagating through a uniform environment, $\mathcal{N} = 0$, and

$$E = \frac{qg'(Fr_i^2 + 2)}{\sqrt[3]{qg'Fr_i^2 r_i^2}}. \tag{8}$$

An important condition is enforced at the front. The nose of an inviscid gravity current or intrusion is conveniently modelled as a jump, for which a relationship between the speed u_N and the height h_N can be derived. Theoretical considerations, supported by experimental and Navier–Stokes simulations ([14], and the references therein) demonstrate that for the present problem the pertinent formula is

$$\frac{dr_N}{dt} = u_N = F\left(g'h_N + \frac{\mathcal{N}^2 h_N^2}{2}\right)^{1/2}, \tag{9}$$

where the generalised Froude number F is a constant close to 1. We note that in an intrusion, $g' = 0$ and (9) simplifies to

$$u_N = \frac{F}{\sqrt{2}}\mathcal{N}h. \tag{10}$$

For a gravity current propagating through an unstratified environment ($\mathcal{N} = 0$),

$$u_N = F\left(g'h\right)^{1/2}, \tag{11}$$

and, in this case, F corresponds to exactly to the Froude number (defined as the ratio of the flow velocity to the gravity wave velocity). There is some uncertainty about the appropriate numerical value of the constant F. Experimental results for a deep unstratified ambient suggest that a practical value is $F = 1.19$ [11], which is bounded from above by the classical result for an ideal fluid flow, $F = \sqrt{2}$ [15].

1.2. Box models

In spite of the apparent simplicity of the axisymmetric shallow water partial-differential equations and associated boundary conditions, analytical solutions are typically not available and the equations must be solved numerically. Numerical solution is complicated by the presence of internal jumps, and in general sophisticated numerical solvers must be used. These complications are exacerbated when there is a source at the axis of symmetry. Furthermore, purely numerical computations do not draw out analytical and asymptotic expressions for the rate of propagation and other key dependent variables. Simplifications are also needed for many practical purposes, and this is what we address in the current contribution.

Very often gravity current motion can be effectively and accurately modelled using 'box models'. These are integral representations of the underlying dynamics and have been applied extensively to gravity currents due to compositional differences with the environment and due to the presence of suspended particles [14,16,17]. For example, applying this standard methodology to a sustained intrusion ($g' = 0$) or gravity current ($\mathcal{N}^2 = 0$), two of the scenarios under investigation in this study, the usual simplification is that the height of the flow does not vary spatially so that the fluid propagates like a cylinder of radius $r_N(t)$ and height $h_N(t)$. Volume continuity, supplemented by the front condition (10), yields the analytical result $r_N = K_{in}(q\mathcal{N}t^2)^{1/3}$ for an intrusion and $r_N = K_{gc}(qg't^3)^{1/4}$ for a gravity current, where K_{in} and K_{gc} are dimensionless constants (see [14], Sections 7.2 and 18.2, and references therein). The success of this approach relies on the motion being quite close to a self-similar form, in which case the neglect of the profile of the height and velocity fields, in favour of an 'averaged' value, still maintains the same dynamic balances as the physical system. The same underlying principle of similarity also underlies 'scaling' analyses that have been applied to these flows to deduce the rate of radial spreading [18,2,19,3]. However, there is strong theoretical evidence [1,20,4], supported by some experimental evidence [2,21] that this approach and the predictions $r_N \sim t^{2/3}$ for intrusions and $r_N \sim t^{3/4}$ for gravity currents are not correct.

The reason for the failure of the box model in axisymmetric, continuously-supplied currents is that the solutions of the shallow-water model are not close to self-similar form [4]. Solutions of the shallow water equations (1)–(3) exhibit a steady thinning region (tail) between the source and some position $r_J(t)$, which expands into a significantly thicker time-dependent annulus (or doughnut-like ring) head. Although the tail region grows in extent as $r_J(t)$ increases with time, within the tail there is no temporal variation of the thickness, velocity or density of the current, and the flow here is therefore in steady state. The occurrence of this shape has been pointed out in gravity currents through unstratified ambients [1,20], in intrusions [22] and for particle-driven currents in an homogeneous ambient [7]; both of the former two cases were analysed more completely by Johnson et al. [4]. Investigations on the steady, but spatially developing states of intrusions [23], and of the unsteady motion [20,4], indicate that the flow in the tail region of both intrusions and gravity currents exhibits a thickness h that decreases as $1/r$ and a radial speed u which is significantly larger than the gravity wave speed $(\mathcal{N}^2 h^2 + g'h)^{1/2}$ and constant in the far-field. There is hence no propagation of information

towards the source because the motion is supercritical ($c_- > 0$). The behaviour in this domain contradicts the assumptions of the classical 'box model'. Since the steady-state flow in this domain controls the influx into the head region, the classical box model approach, which is based on a control volume with homogeneous time-dependency for the entire current, becomes inadequate. We clearly need a different simplification.

We now face two major questions: (1) what is the location $r_J(t)$ of the boundary between the steady inner tail and annular head (see Fig. 1)? The steady-state solution provides h, u as functions of r in a quite simple way, but it does not provide any indication of the domain of relevance at a given time t; (2) what is the flow in the time-dependent domain close to the front of the current? It is evident that such a domain must exist, because the steady-state solution cannot be matched to the front condition (9). In particular, it is important to be able to predict the propagation of the front, $r_N(t)$, and the volume of fluid in the time-dependent domain. One means for obtaining this information is by the numerical solution of the shallow water equations, as done in [4]. This is an accurate, but not a straightforward, method.

Here we derive a simple approximate solution, in the spirit of the box model. Due to its simplicity, this model is particularly convenient for applications and yet reveals considerable insight into the underlying motion and is consistent with predictions from the more complete shallow water equations. First, we consider the motion of a homogeneous intruding fluid (Section 2) and then a homogeneous gravity current propagating through a uniform ambient (Section 3). At a later stage, we allow the intrusion to contain a dilute suspension of settling particles, such as ash particles as for a volcanic intrusion, and we determine the influence of the motion on the distribution of the particles (Section 4.1). We analyse sustained particle-driven flows (Section 4.2) and, finally, present a short summary of the new hybrid model in Section 5.

2. A hybrid model for intrusions

We introduce a new model that is motivated by the numerically computed and asymptotic solutions of the shallow water partial-differential-equations [4] and yet the new approach retains many of the simplifying features of box models. The solution realised by the full system of equations has two distinct domains. In the domain from the source to $r_J(t)$, the flow is steady, and is given by a steady-state solution of the shallow water equations. At the front of the current, in the domain $r_J(t) \leq r \leq r_N(t)$, the flow variables are time-dependent and weakly spatially varying. For our new hybrid model, we assume that the radial gradients of the depth-integrated hydrostatic pressure field vanish across the frontal region, because they are otherwise unbalanced in the radial momentum equation on sufficiently short lengthscales, close to the front. Thus for an intrusion, this implies that there are no spatial gradients of the height field sufficiently close to the front; the flow here takes the shape of an annulus of thickness $2h_N(t)$ (see Fig. 1). The two domains are connected by a jump at $r = r_J(t)$, across which the current expands from a half-thickness h_{J-} to $h_{J+} = h_N$, where the latter is the depth at the front. The idea of this model is that the steady shallow water solution in the $r \leq r_J(t)$ domain is simple, and hence approximations are made only in the $r_J(t) < r \leq r_N(t)$ domain.

We orientate the coordinate axes so that z is vertical and $z = 0$ is the neutral buoyancy line. Since the stratification of the environment is constant ($\mathcal{N}^2 =$ constant), the intrusion spreads symmetrically about $z = 0$ and has thickness $2h$. Recalling that the flow is driven by a sustained volume flux per unit radian q in the upper half of the intrusion, we introduce a dimensional length scale $[q/\mathcal{N}]^{1/3}$ and time scale $1/\mathcal{N}$, and henceforth use these two to render all of the variables dimensionless.

2.1. The steady-state domain ($r_i < r < r_J(t)$)

Here we use the exact steady solution of the shallow water equations (1) and (2), rendered dimensionless as described above. Together these admit the constants of the motion

$$hur = 1 \quad \text{and} \quad h^2 + u^2 = C_0^2, \tag{12}$$

which represent mass conservation and the dimensionless energy constant (see (7)). As described above, the constant C_0^2 is prescribed by the boundary conditions h_i, u_i at the inner radius r_i and is given by $C_0^2 = (1 + Fr_i^2)/(r_i Fr_i)$. After some algebra we obtain explicit expressions for $h(r)$ and $u(r)$,

$$u^2 = \frac{1}{2}\left[C_0^2 + \sqrt{C_0^4 - 4/r^2} \right]; \tag{13}$$

$$h^2 = \frac{1}{2}\left[C_0^2 - \sqrt{C_0^4 - 4/r^2} \right] = \frac{2}{C_0^2 r^2 + \sqrt{(C_0^2 r^2)^2 - 4r^2}}; \tag{14}$$

(the latter form is useful for numerical computations and avoids cancellation errors when r is large). The solutions (13) and (14) are supercritical. There is an additional steady subcritical solution but this is not realised by the flows under consideration here. The steady-state h, u used here are consistent with the results of Baines [23], but the novelty here is the realisation that this solution must be joined to a region of unsteady evolution at the front. Furthermore, it turns out that the tail contains only a relatively small part of the influxed volume.

The dimensionless volume of the tail region per unit radian is

$$\mathcal{V}_1(t) = \int_{r_i}^{r_J(t)} h(r)r \, dr. \tag{15}$$

Since $h(r)$ is given explicitly by (14), the integral is easily evaluated when needed (we did this numerically, because the analytical formula is awkward). We emphasise that this volume increases with time because r_J increases. However, since the entire volume of the intrusion increases like t, the proportion of fluid in the tail region is $\mathcal{V}_1(t)/t$; as shown below, this is a decreasing function.

The domain from the axis $r = 0$ to r_i is not treated in this model as the source is assumed to be at the inlet radius r_i. The constant C_0^2 is a boundary condition; it takes the value 2 when the flow is critical ($Fr_i = 1$) at $r_i = 1$. We conclude that the flow in the tail is known, and provided by simple formulae. However to make this solution useful, we must determine the outer radius $r_J(t)$ of this domain. This requires the solution of the head domain, as shown below.

2.2. The head region ($r_J(t) < r < r_N(t)$)

We consider now the region from $r_J(t)$ to $r_N(t)$, in which we have introduced the simplification that the intrusion is of constant thickness $2h_N(t)$ (see Fig. 1). This is the major simplification in our description and is where this hybrid model shares some features with 'box' models. Under this simplification, volume continuity in the upper half of the intrusion yields

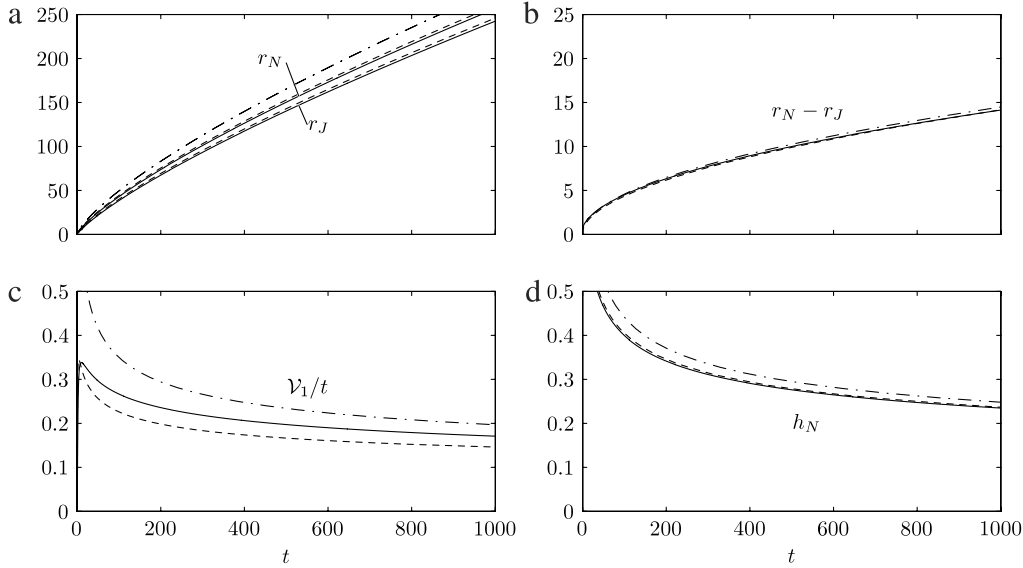$$\frac{1}{2}\left[r_N^2(t) - r_J^2(t) \right] h_N + \mathcal{V}_1(r_J) = t \tag{16}$$

and hence

$$h_N = 2(t - \mathcal{V}_1(r_J))/[r_N^2(t) - r_J^2(t)]. \tag{17}$$

This leaves two unknowns, $r_N(t)$ and $r_J(t)$. The first one is determined from the front condition (10), which in dimensionless form is given by

$$\frac{dr_N}{dt} = \frac{F}{\sqrt{2}} h_N. \tag{18}$$

Fig. 2. The positions of the front, $r_N(t)$ and shock, $r_J(t)$, the height of the front, h_N, the width of the front, $r_N - r_J$ and the proportion of the volume of fluid in the steady tail $\mathcal{V}_1/t$ as functions of time, for an intrusion. Here, and throughout this paper, hybrid model solutions are indicated by solid curves and shallow water solutions by dashed curves. The leading-order asymptotic estimates for $t \gg 1$ (derived in Section 2.4) are indicated with a dash-dotted curve.

We recall that r_J is the position of the jump; the conditions u_{J^-} and h_{J^-} at $r = r_{J^-}$ are provided by the steady-state solution (13) and (14). Denoting the speed of the jump by $c \equiv dr_J/dt$, we express volume and momentum balances across the jump to find $dr_J/dt = \max(0, c)$, where (see Appendix A)

$$c = u_{J^-} - \left[\frac{1}{3} \frac{h_N}{h_{J^-}} (h_N^2 + h_{J^-}^2 + h_N h_{J^-}) \right]^{1/2}. \tag{19}$$

Here we impose $dr_J/dt \geq 0$ to avoid unphysical inward propagation, which may otherwise occur during the initial phases. This inward propagation results from the discrepancy between the shallow-water model, which predicts some spatial variation within the head region at very early times [4], and the hybrid model assumption that the head is of uniform thickness. For given initial conditions r_J and r_N, we can calculate the subsequent propagation by a simple numerical integration of the ODEs (18) and (19), and the intrusion thickness at the front $2h_N(t)$ is a by-product of this calculation.

The input parameters of the model are: at the source $r = r_i$, and $u_i/h_i = Fr_i$, and $h_i u_i r_i = 1$; at the nose $r = r_N$, $u_N/h_N = F$. Unless stated otherwise, in figures we use $r_i = Fr_i = 1$, and $F = 1.19$. In Section 2.4 we will calculate the dependence of the flow at large times on these parameters, and show in particular that the dependence on the initial radius r_i is remarkably weak, with r_N scaling as $r_i^{-1/8}$. It is convenient to start the calculation with $r_N = r_J = r_i$, and $h_N = h_i$ at $t = 0$.

2.3. Comparison with solutions of the shallow-water model

In Fig. 2 we compare the results from our hybrid model with those computed numerically from the shallow water equations, using the same non-oscillatory numerical scheme as Johnson et al. [4]. The agreement is very good over a long time of propagation, $t = 10^3$. (For an intrusion in the atmosphere, $\mathcal{N} = 0.01 \text{ s}^{-1}$, and a dimensionless time of $t = 10^3$ corresponds to about 28 h of propagation and for application to a volcanic source, this corresponds to a long duration eruption.) The absolute discrepancy between the models for r_N increases with time, but is less than 2% at $t = 10^3$; furthermore, the relative error diminishes. Both the shallow water solution and the hybrid model predict that most of the

volume is in the head region. At $t = 10^3$, the tail contains only 17% of the volume according to the hybrid model (and 15% according to the shallow water solution). Comparisons between results generated with other input parameters show similar agreement between the model and shallow water predictions.

2.4. Long-time asymptotes

Analysis of the governing shallow-layer equations indicates that when $t \gg 1$ the propagation is such that the intrusion radius r_N grows as $t^{3/4}$ [4]. We show that this carries over to the hybrid model; moreover, a simple calculation of the coefficient multiplying this power of time is possible.

We postulate that for sufficiently long times ($t \gg 1$), the leading terms behave like

$$r_N = Kt^\beta; \qquad r_N - r_J = Dt^\gamma \tag{20}$$

where K, D, β, γ are positive constants, which will be determined. Physical considerations indicate that $\beta < 1$ (otherwise the nose accelerates to infinity). Our model assumes that the head is a thin annulus, and hence we assume (and later confirm) that $\beta > \gamma$. This implies that $(r_N - r_J)/r_N \ll 1$. We keep in mind that large t also means large r_J and r_N.

For $r \gg 1$, from (12), (13), and (20), we obtain, to leading order,

$$u_{J^-} = C_0 \quad \text{and} \quad h_{J^-} = 1/(u_J - r_J) = 1/(C_0 r_N). \tag{21}$$

We now analyse the speed of the jump at r_J, (19). The first term on the RHS, u_{J^-}, is now a constant. However, in view of (20), dr_J/dt behaves like dr_N/dt, which is expected to decay like $t^{\beta-1}$. Consequently, to leading order, the second term on the RHS of (19) must cancel the first one. We also expect that h_N dominates h_{J^-} (this is confirmed by (25) below). Therefore, (19) produces the balance

$$u_{J^-}^2 = (1/3)h_N^3/h_{J^-}, \tag{22}$$

rewritten, using (21), as

$$3C_0 = h_N^3 r_N = h_N^3 Kt^\beta. \tag{23}$$

On the other hand, the front condition is

$$\frac{dr_N}{dt} = \beta Kt^{\beta-1} = \frac{F}{\sqrt{2}} h_N, \tag{24}$$

or

$$h_N = (\sqrt{2}/F)\beta K t^{\beta - 1}. \tag{25}$$

We substitute this h_N into (23). Equating powers of t and the coefficients, we obtain

$$\beta = \frac{3}{4}; \qquad K^4 = 3C_0 \left(\frac{F}{\sqrt{2}\beta}\right)^3. \tag{26}$$

This prediction of our simple model is in good agreement with very recent experimental findings [21].

To determine D and γ we use the volume equation (per radian) in the annulus of height h_N about r_N

$$h_N r_N (r_N - r_J) = h_N r_N D t^\gamma = t, \tag{27}$$

where the last term is the volume supplied by the source. Substitution of r_N, h_N in terms of K, t, β, and some algebra, yield

$$\gamma = \frac{1}{2}; \qquad D = \frac{F}{\sqrt{2}\beta} K^{-2}. \tag{28}$$

This validates our initial assumption that $\beta > \gamma$ and so $r_N \sim t^{3/4}$, while $r_N - r_J \sim t^{1/2}$.

In (27) we assumed that there is no significant volume in the tail (as compared to the total volume, which increases in proportion to t). The justification is as follows. The thickness of the tail behaves like $1/(C_0 r)$, see (21). We can thus estimate the relative amount of the volume in the tail, as

$$\frac{\mathcal{V}_1}{t} = \frac{1}{t} \int_{r_i}^{r_J} h r \, dr = \frac{K}{C_0} t^{-1/4} + \cdots, \tag{29}$$

where r_i was neglected, and $r_J = r_N = K t^{3/4}$ was used. Thus $\mathcal{V}_1/t$ diminishes as t increases (see Fig. 2(c)).

The leading-order asymptotic behaviour of the hybrid model derived in this section is compared in Fig. 2 to numerical solutions of the hybrid model. The trends $t^{3/4}$ and $t^{1/2}$ for r_N and extent of the annulus $r_N - r_J$ are observed from quite early times, say $t > 10$.

We note that the coefficients K and D are the same as those found for the complete late-time solutions to the full shallow-water model [4]. This reflects the fact that the annulus, chosen as a simplification for the shape of the head region in the hybrid model, is in fact the leading-order shape of the head region at late times in solutions to the full shallow-water governing equations. In terms of the dynamics, it confirms that sufficiently close to the front $((r_N - r)/r_N \ll 1)$, which corresponds to the entire frontal region when $t \gg 1$, gradients of depth-integrated hydrostatic pressure vanish. We note also the counterintuitive dependence of K on the inflow radius r_i (given). For a constant volume flux and Froude number at source, from (7) and (26) we determine that $K \sim r_i^{-1/8}$, that is, that the current radius at large times is a weakly decreasing function of the source radius.

In summary, for $t > 10$, the motion predicted by the model can be well approximated by the following simple lines. Recalling that F refers to the generalised Froude number that enters into the frontal boundary condition (10), the nose propagates with $r_N = K t^{3/4}$, the height is $[3\sqrt{2}/(4F)]K t^{-1/4}$, and the thickness of the annulus is $D t^{1/2}$, where K, D are given by the simple expressions (26) and (28). The relative amount of volume in the tail is fairly well estimated by (29). The powers of t are universal; the boundary conditions influence only the coefficients.

3. A hybrid model for gravity currents

Solutions of the shallow-water governing equations (1) and (2) for gravity currents ($g' > 0$) exhibit similar qualitative features to those of intrusions, namely a tail region in which the flow is steady, connected through a shock to a time-dependent head region at the flow front (see, for example, the computations of Slim and Huppert [20] when $\mathcal{N}^2 = 0$). We therefore construct a similar hybrid model to that obtained for intrusions in the previous section, for gravity currents flowing beneath a stratified or unstratified environment.

When considering gravity currents we render the variables dimensionless with respect to a lengthscale $(q^2/g')^{1/5}$ and timescale $(q/g'^3)^{1/5}$. In the steady-state 'tail', the continuity and momentum equations (1) and (2) in dimensionless form are

$$hur = 1; \quad \text{and} \quad u^2 + 2h + \sigma h^2 = A_0^2 \tag{30}$$

which represent the constant mass flux and the Bernoulli constant, respectively. Here $\sigma \equiv \mathcal{N}^2 q^{2/5}/g'^{6/5}$ measures the dimensionless strength of the stratification.

As before, A_0 can be expressed in terms of a Froude at source and the dimensionless radius at which the source conditions are applied. Hence $u(r)$, $h(r)$ are given by the equations

$$u^4 - A_0^2 u^2 + \frac{2u}{r} + \frac{\sigma}{r^2} = 0; \qquad h = \frac{1}{ur}. \tag{31}$$

An analytical solution to (31) is available, but a numerical Newton–Raphson iterative calculation of the relevant root is more convenient. Since we consider the domain $r > r_i$, with a typical value $A_0^2 = 3 + \sigma$, a good starting value for the iterations is to use the first two terms of the large r approximation, $u = A_0[1 - 1/(A_0^3 r)]$; then, convergence to six–seven digits is achieved in 2–3 iterations. As in the case of an intrusion, a steady flow is realised within a tail region, between $r = r_i$ and $r = r_J(t)$, and the volume per unit radian of this steady-state domain is given by $\mathcal{V}_1(t)$ (15). Using (30) and (31), this volume may be evaluated numerically.

Under the construction of the hybrid model, the annulus from $r_J(t)$ to $r_N(t)$ is of height $h_N(t)$ and, as with the case of intrusions, volume continuity yields the expression for h_N given by (17). The unknown $r_N(t)$ is determined from the front condition (9), which in nondimensional form is

$$\frac{dr_N}{dt} = u_N = F\left(h_N + \frac{\sigma h_N^2}{2}\right)^{1/2}. \tag{32}$$

We recall that r_J is the position of the jump; the conditions u_{J-} and h_{J-} at r_{J-} are provided by the steady-state solution at $r = r_J$. In a frame moving with the speed of the jump ($c = dr_J/dt$), we write the volume and momentum balances; see Appendix A. After some algebra, we obtain an equation for the second unknown $r_J(t)$, $dr_J/dt = \max(0, c)$, where

$$c = u_{J-} - \left[\frac{h_N}{h_{J-}}\left(\frac{1}{2}(h_N + h_{J-}) + \frac{\sigma}{3}\left(h_N^2 + h_N h_{J-} + h_{J-}^2\right)\right)\right]^{1/2}. \tag{33}$$

Given initial conditions for r_J and r_N, we calculate the subsequent propagation by numerically integrating of (32) and (33). The source conditions are similar to the stratified model: $u_i = r_i = h_i = 1$, which gives $A_0^2 = 3 + \sigma$ and we start the temporal integration from $r_N = r_J = r_i$.

The behaviour of this form of the hybrid model is rather similar in character to the case of intrusions. In particular the hybrid model is capable of accurately reproducing the results of a more complete numerical integration of the shallow water equations but with much simpler and faster numerical methods. Comparisons to the shallow water solutions show very good agreement, see Fig. 3; here we have shown the detailed comparisons for $\sigma = 0$, but other values yield similarly good agreement.
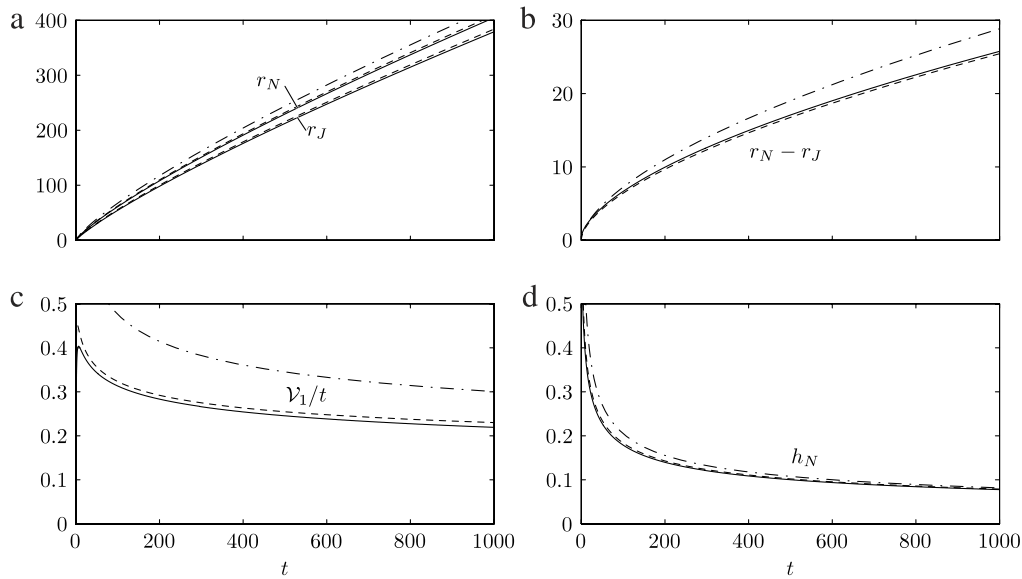
Fig. 3. The positions of the front, $r_N(t)$ and shock, $r_J(t)$, the height of the front, h_N, the width of the front, $r_N - r_J$ and the proportion of the volume of fluid in the steady-state tail $\mathcal{V}_1/t$ as functions of time for gravity current propagation through an unstratified ambient ($\sigma = 0$). The hybrid model is indicated by solid curves, the shallow water model by dashed curves, and the leading-order asymptotic expressions for large t as dash-dotted curves.

3.1. Long-time asymptotes

We use the hybrid model to draw out the long time behaviour of sustained axisymmetric gravity currents in a homogeneous ambient, $\mathcal{N} = 0$ (or for small σ). The analysis proceeds in an analogous way to that for intrusions in Section 2.4. To this end we pose

$$r_N = Kt^\beta, \qquad r_N - r_J = Dt^\gamma, \tag{34}$$

where K, D, β, γ are positive constants to be determined. As before we argue that $\gamma < \beta < 1$.

For large r_J, using an expansion in powers of $(1/r)$ for (30) and (31), we obtain, to leading order,

$$u_{J^-} = A_0; \quad \text{and} \quad h_{J^-} = 1/(u_{J^-} r_J) = 1/(A_0 r_N). \tag{35}$$

We now consider the shock speed (33). The first term on the RHS, u_{J^-}, is now a constant. However, in view of (34), c must behave like dr_N/dt, which is expected to decay with t. Consequently to leading order, the second term in (33) must cancel the first one. We also expect that $1 \gg h_N \gg h_{J^-}$ at large t (this is confirmed below). The inequality $1 \gg h_N$ means that, at large times, terms resulting from the stratification of the ambient are negligible compared to those resulting from the difference in density between the current and ambient ($\rho_c - \rho_0$). At late times, (33) therefore produces the balance

$$u_{J^-}^2 = (1/2)h_N^2/h_{J^-}, \tag{36}$$

rewritten, using (35) as

$$2A_0 = h_N^2 r_N = h_N^2 K t^\beta. \tag{37}$$

On the other hand, the front condition, for large times when $h_N \gg \sigma h_N^2/2$, is

$$\frac{dr_N}{dt} = \beta K t^{\beta-1} = F h_N^{1/2}, \tag{38}$$

or

$$h_N = (\beta K/F)^2 t^{2\beta-2}. \tag{39}$$

We substitute this h_N into (37). Equating powers of t and the coefficients, we obtain

$$\beta = \frac{4}{5}; \qquad K^5 = 2A_0 \left(\frac{F}{\beta}\right)^4. \tag{40}$$

To determine D, γ we use the volume equation (per radian) in the annulus of height h_N about r_N

$$h_N r_N (r_N - r_J) = h_N r_N D t^\gamma = t; \tag{41}$$

where the last term is the volume supplied by the source. Substitution of r_N, h_N in terms of K, t, β yields

$$\gamma = \frac{3}{5}; \qquad D = \frac{F^2}{\beta^2} K^{-3}. \tag{42}$$

This validates our initial assumption that $\beta > \gamma$. Furthermore we note that the relative amount of volume in the tail, $\mathcal{V}_1/t$, is given by $(K/A_0)t^{-1/5}$.

The results $r_N = Kt^{4/5}$ and $h_N = (\beta K/F)^2 t^{-2/5}$ are in full agreement with the long time behaviour of the shallow water solution [20,4]. The asymptotes are also in good agreement with the numerical solution of the hybrid model. In all tested cases, the time powers $\beta = 4/5$ and $3/5$ for r_N and $r_N - r_J$ are evident after $t = 50$. The coefficients are also quite sharp. For example, for the case $h_i = u_i = r_i = 1, F = 1.19$, the prediction is $K = 1.762, D = 0.405$; the numerical results at $t = 10^3$ are 1.611, 0.408, respectively. At this time the tail still contains about 22% of the volume.

3.2. Comparison with solutions of the shallow-water model

In Fig. 4 we plot the position of the radial front as a function of time for gravity currents through ambients with stratifications characterised by $\sigma = 0, 2$ and 10. In terms of the dimensionless variables used here, the stratification always enhances the rate of propagation during the initial phases, but at late times the current has become sufficiently thin so that it is not strongly affected by the density variation within the ambient itself. From (32) and (40) we may assess a dimensionless timescale at which the effects of the stratification begin to diminish; this is given by $\sigma h_N \sim 1$ and thus $t \sim \sigma^{5/2}$.
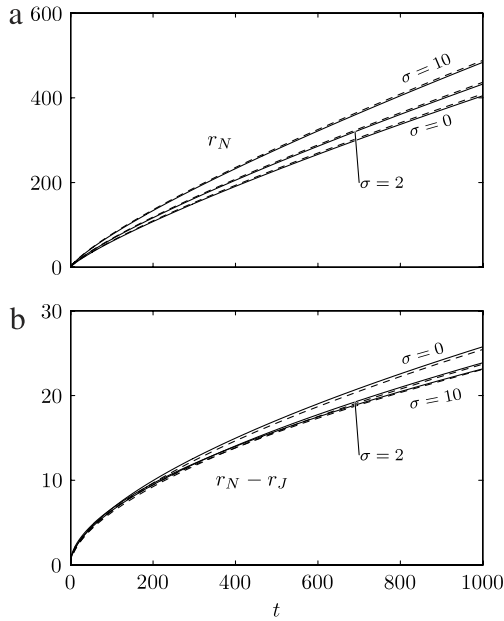
Fig. 4. (a) The position of the front r_N, and (b) the width of the frontal region $r_N - r_J$, as functions of time for gravity currents propagating through an ambient with dimensionless stratification $\sigma = 0$, 2 and 10. Hybrid model results are indicated by solid curves, and shallow water solutions by dashed curves.

4. Particles: transport and sedimentation

We now analyse the transport of suspensions of relatively dense particles by these flows. In particular we examine two regimes; the first is when the concentration of particles is sufficiently dilute so that their presence does not significantly alter the bulk density. This regime is relevant to sustained horizontal intrusions of volcanic ash clouds, and to this end we analyse particle transport and settling when the flow dynamics are given by the hybrid model as in Section 2. The second problem analysed here is when the presence of the particles alone determines the excess density of the current which moves through an otherwise uniform environment. For this 'particle-driven' case the dynamics of the current are strongly coupled to the evolution of the volume fraction of particles. For both situations we demonstrate that the hybrid model is an effective tool for calculating the transport of particles and accumulation of the deposit with negligible computational effort.

4.1. Particle-laden intrusions

Motivated by the application of the hybrid model for intrusions to the motion of volcanic ash clouds, we limit the analysis to the case of intrusions, and note that for the regimes discussed here, the result for gravity currents is entirely analogous. We assume that the volume fraction of the dispersed particles is small enough that the contribution of particles to the bulk density is small, and hence they are carried by the intrusion without affecting the dynamics of the propagation. The simplest case is of a single dispersed species: the volume fraction of particulate at the source, assumed constant, is denoted by ϕ_0, and the dimensionless settling speed, scaled against $(q\mathcal{N}^2)^{1/3}$, is w_s, approximately 10^{-4}–10^{-2} for particles 10–100 μm in diameter in a typical volcanic plume.

In what follows, we compute the volume fraction of the particles $\phi(r, t)$, scaled by its value at source ϕ_0. We model the particle transport and settling on the assumption that the intrusion is sufficiently turbulent to maintain a well-mixed layer of particles, but that the particles settle out over the lower interface of the intrusion. In view of the flow-field given by the hybrid model,
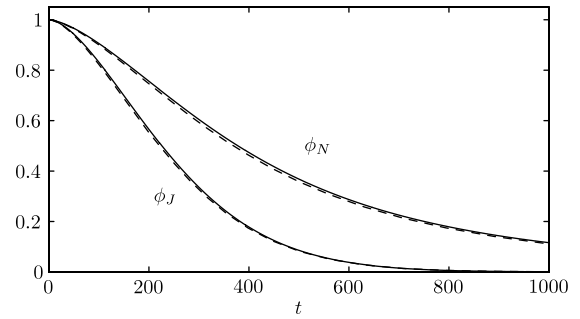
Fig. 5. The particle volume fraction ϕ_{J-} at $r = r_J$ and the average volume fraction in the head ϕ_N, as functions of time, for a particle-laden intrusion with $w_s = 5 \times 10^{-4}$. The hybrid model results are shown by solid curves and the shallow water results by dashed curves.

the particle distribution has also two domains. The first domain, $r_i \le r \le r_J(t)$, leads to a steady-state $\phi(r)$. In the second domain, $r_J(t) < r < r_N(t)$, we assume a time-dependent volume fraction, representative of the entire frontal region ($\phi_N(t)$).

The particles settle out from the lower boundary of the intrusion. Therefore, the height under concern is $2h$ of the 'upper half' solved above (Fig. 1), and the scaled volume flux is $2rhu = 2$. In the tail domain we use, again, the steady-state shallow layer equations, in particular (3), which takes the dimensionless form

$$\frac{1}{r} \frac{\mathrm{d}}{\mathrm{d}r} (2hur\phi) = -w_s \phi(r). \tag{43}$$

The solution, subject to $ruh = 1$, is

$$\phi(r) = \exp\left(-\frac{1}{4} w_s (r^2 - r_i^2)\right) \quad (r_i \le r \le r_J(t)). \tag{44}$$

This Gaussian concentration profile is in good agreement with the existing steady-state theory [24].

For the time-dependent head domain, of volume $\mathcal{V}(t) = t - \mathcal{V}_1(t)$, we need a conservation equation to determine the concentration within the frontal region. Under the assumptions of the hybrid model for these dilute intrusions, the height of the frontal region is spatially invariant and so too is the volume fraction of particles, $\phi_N(t)$. The volume of particles, $\phi_N(t)\mathcal{V}(t)$, changes because: (a) there is influx of suspended particles at r_J, with speed $u_{J-} - c$, into the head domain; and (b) there is settling of particles out of the lower boundary of the head domain. This we write as

$$\frac{\mathrm{d}}{\mathrm{d}t} (\phi_N \mathcal{V}) = h_{J-} \left(u_{J-} - c\right) r_J \phi_{J-} - \frac{w_s \phi_N \mathcal{V}}{2h_N}. \tag{45}$$

This particle conservation equation is closed by integrating it alongside the existing hybrid model equations for an intrusion, (18) and (19), which govern the evolution of the location and speed of the shock, r_J and c. We note that if no sedimentation ($w_s = 0$) Eq. (45) implies that ϕ_N remains equal to its value at source everywhere, and (45) then reduces to the volume conservation within the head region. This hybrid model formulation for the conservation of particles within the frontal region is able to reproduce accurately the results of the more complete shallow layer equations [4] (see Fig. 5).

We note that this procedure can be easily extended to several species: under the assumption that there is no interaction between species, the hybrid model equations (44) and (45) are simply augmented with a particle conservation equation (45) for each species of particles, each with the appropriate w_s and ϕ_0.

The volume flux per unit area of the particles which settle out at position r at time t is $w_s \phi_0 \phi_N(r, t)$, for $r \le r_N(t)$ (and of course
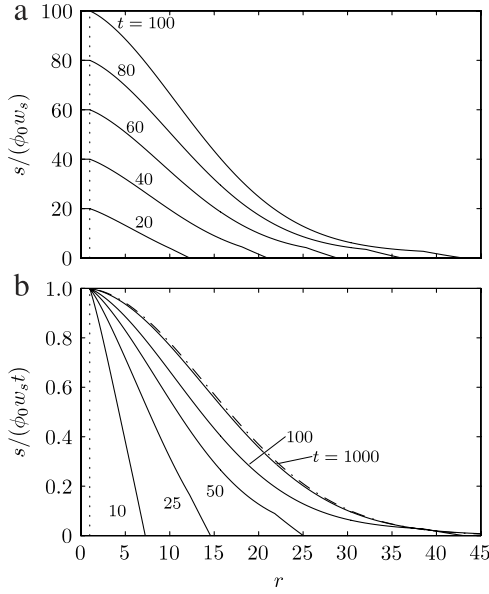
Fig. 6. (a) The distribution of the deposit, $s(r, t)$ as a function of radial distance as various instances of time, arising from settling from a particle-laden intrusion with a nondimensional velocity $w_s = 10^{-2}$ and $\phi_M = 1$. (b) The distribution of the deposit scaled by the time elapsed, $s(r, t)/t$. The long-time scaled distribution for the deposit, $\exp(-w_s(r^2 - r_i^2)/4)$, is plotted as a dash-dotted line. Vertical dotted lines depict the initial radius of the intrusion.

zero at larger radii). Consequently, the thickness of the sediment $s(r, t)$ is given by

$$s(r, t) = \frac{\phi_0 w_s}{\phi_M} \int_{t_s}^{t} \phi(r, t') \, dt', \tag{46}$$

where t_s is the starting time for settling at a dimensionless distance r from the origin, given by $r_N(t_s) = r$ and ϕ_M is the volume fraction corresponding to maximum packing within the deposit. With the values of $\phi(r, t)$ provided by the hybrid model, the numerical calculation of $s(r, t)$ is straightforward; and example is illustrated in Fig. 6. Apart from within the head of the intrusion, the volume fraction ϕ attains the steady distribution given by (44). At relatively long times (when $w_s^{1/2} r_J(t) \gg 1$), most of the deposition from the intrusion occurs in steady tail region, and thus we anticipate that deposit will reflect the steady distribution (44). This is confirmed by numerical calculations of the deposit thickness (Fig. 6(b)).

4.2. Particle-driven currents through uniform environments ($\sigma = 0$)

The dynamics of particle-driven currents are more complex because progressive settling of the particles reduces the driving gravitational force. The solution can be obtained as follows. First, the steady equation (3) for the volume fraction $\phi(r)$, with $d = h(r) = 1/(u(r)r)$ is integrated and yields the dimensionless

$$\phi(r) = \exp\left[-\frac{w_s(r^2 - r_i^2)}{2}\right], \qquad \phi'(r) = -w_s r \phi(r), \tag{47}$$

where the prime denotes a derivative with respect to r.

The momentum equation (2) for the steady tail is expressed, in dimensionless form, as

$$uu' + \phi h' + \frac{1}{2} h \phi' = 0. \tag{48}$$

Using $hur = 1$, after some manipulation we obtain

$$h' = \frac{h - \frac{1}{2}(hr)^3 h \, \phi'}{(hr)^3 \phi - r}. \tag{49}$$

From (15), the volume of the tail satisfies

$$\mathcal{V}_1'(r) = hr. \tag{50}$$

The numerical integration of (49)–(50), aided by (47) and $hur = 1$, provides the needed variables in the steady tail. When $r_i = u_i = h = 1$, h' is singular at this point, so we start the integration with the approximation $Fr_i = 1.0001$ at $r = 1$. In general, $u(r)$ increases with r to a constant, h decreases $\sim 1/r$, and $\mathcal{V}_{\text{tail}} \sim r_J$. More details will be given later.

We proceed by forming evolution equations for the radial positions of the front and the shock, the volume fraction of particles within the frontal region, ϕ_N and the volume of fluid within the frontal region $\mathcal{V} = (r_N^2 - r_J^2)h_N/2$, which are all assumed to be functions only of time. Conservation of fluid mass is then expressed by

$$\mathcal{V}_1(r_J) + \mathcal{V} = t, \tag{51}$$

while the dynamic condition at the front is given by

$$\frac{dr_N}{dt} = F \left(\phi_N h_N\right)^{1/2}. \tag{52}$$

Settling of particles follows the conservation law above (45) and in this context is given by

$$\frac{d}{dt} \left(\phi_N \mathcal{V}\right) = h_{J-} \left(u_{J-} - c\right) r_J \phi_{J-} - \frac{w_s \phi_N \mathcal{V}}{h_N}. \tag{53}$$

This may be re-written to express the evolution of ϕ_N, as

$$\frac{d\phi_N}{dt} = -\frac{w_s \phi_N}{h_N} - \frac{d\mathcal{V}}{dt} \frac{(\phi_N - \phi_{J-})}{\mathcal{V}}. \tag{54}$$

Finally a jump condition is used to determine the shock speed $dr_J/dt = \max(0, c)$ (see Appendix A),

$$c = u_{J-} - \left[\frac{h_N}{2h_{J-}} \left(\frac{\phi_N h_N^2 - \phi_{J-} h_{J-}^2}{h_N - h_{J-}}\right)\right]^{1/2}, \tag{55}$$

where the conditions at $r = r_{J+}$ have been replaced with the time varying, but spatially uniform quantities within the frontal region. We integrate the system of coupled differential equations from initial conditions $r_N = r_J = r_i = 1$, $\phi_N = 1$. The agreement between the hybrid model and the shallow water model is very good for a range of dimensionless settling velocities (Fig. 7).

The use of the hybrid model to analyse the dynamics of sustained, radially spreading, particle-driven gravity currents draws out the key feature of their unsteady evolution. They feature a tail within which the volume fraction $\phi(r)$ is in steady state and decays exponentially with r^2 (44), coupled to an unsteadily evolving front. Within this front, which is fed by the steady tail, the time-dependent volume fraction decays due to sedimentation and dilution by the influxed fluid; this balance is encompassed mathematically by (54). The existence of the unsteady front is due to the retardation of the current, here encapsulated through the imposition of a Froude number of order unity at the front of the motion (52). There are thus potentially different lengthscales pertinent to the motion within the steady-state tail and the unsteady front.

4.3. Long-time behaviour

In the steady-state tail, significant sedimentation occurs over a dimensionless lengthscale $w_s^{1/2} r$, which is the e-folding lengthscale of the volume fraction of suspended particles (see (44)). In the regime of a relatively small dimensionless settling velocity ($w_s \ll 1$), which is the regime of usual physical interest, the height and
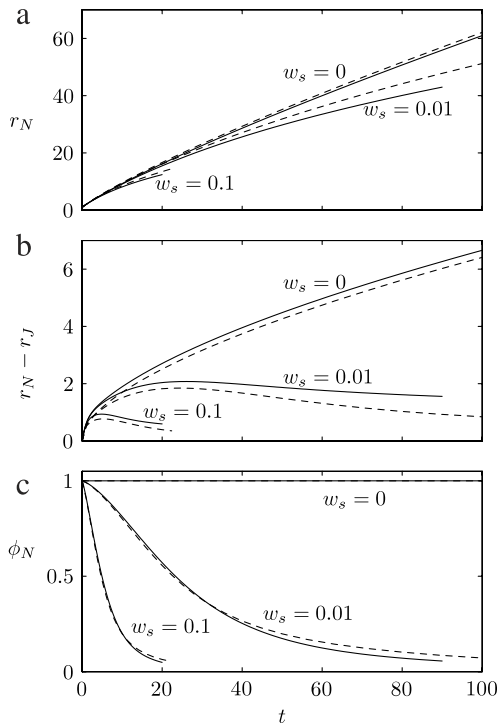
Fig. 7. The position of the front, $r_N(t)$, the width of the frontal region, $r_N - r_J$ and the volume fraction of the front, ϕ_N as a function of dimensionless time for $w_s = 0$, 0.01 and 0.1. The solid line corresponds to the hybrid model; the dashed line to computations of the complete shallow layer model.

velocity fields may be shown to satisfy (see Appendix B)

$$u^2 + 2\phi h = A^2 \equiv \left(A_0^3 - w_s^{1/2} \frac{3}{2} \int_0^{w_s^{1/2}r} \exp(-s^2/2)\, \mathrm{d}s \right)^{2/3}. \quad (56)$$

Furthermore when $r \gg 1$, $u = A$ and $h = 1/(Ar)$ and

$$A^3 \to A_\infty^3 \equiv A_0^3 - w_s^{1/2} \frac{3\sqrt{\pi}}{2\sqrt{2}} \quad \text{as } r \to \infty. \quad (57)$$

In the unsteady frontal region, we rescale the dimensionless variables by writing

$$r_N = R_\infty \hat{r}, \qquad t = T_\infty \hat{t},$$
$$h = H_\infty \hat{h} \quad \text{and} \quad r_N - r_J = T_\infty (H_\infty R_\infty)^{-1} \hat{\delta}, \quad (58)$$

where the latter scaling for the width of the frontal region is chosen to ensure that the rescaling of the front is consistent with mass conservation (51). For balance in the settling Eq. (54), we choose $H_\infty = w_s T_\infty$, while for balance in the dynamic equation (52), we choose $R_\infty = FT_\infty H_\infty^{1/2}$. To complete the rescaling we require one further condition. One possibility is to assume that the radial lengthscale is determined by the e-folding decay length of the volume fraction (44), so that $R_\infty = w_s^{-1/2}$. However this is inconsistent with the jump condition between the steady and unsteady regions (55). Instead, since $\phi_N h_N^2 \gg \phi_{J^-} h_{J^-}^2$ and $h_N \gg h_{J^-}$, we find that to leading order,

$$u_{J^-}^2 h_{J^-} = \frac{1}{2} \phi_N h_N^2 + \cdots \quad (59)$$

and thus using (56), we choose $H_\infty^2 = A_\infty / R_\infty$. The length and time scales relevant to the unsteady front are thus given by

$$R_\infty = \left(\frac{F^4 A_\infty^3}{w_s^4} \right)^{1/7} \quad \text{and} \quad T_\infty = \left(\frac{A_\infty^2}{w_s^5 F^2} \right)^{1/7}. \quad (60)$$
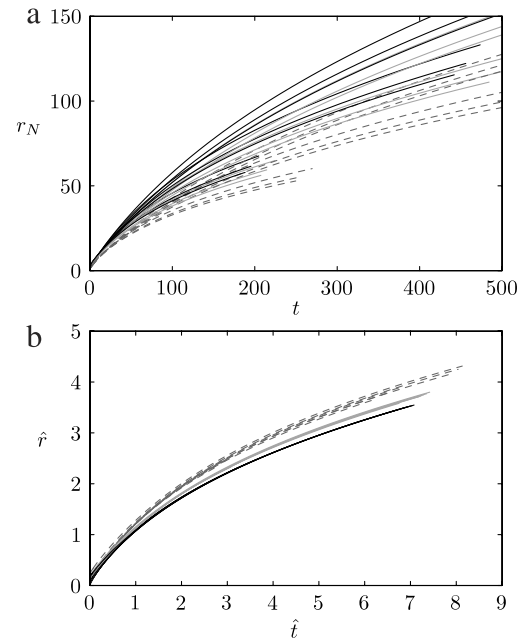

Fig. 8. (a) The front position, r_N as a function of t for a range settling velocities, Froude numbers and source radii; (b) the rescaled front position, $\hat{r}$ as a function of rescaled time $\hat{t}$. The curves are coded according to the value of the Froude number; $F = 1.19$ (black); $F = 1$ (grey solid); and $F = 0.72$ (grey dashed).

We have integrated the hybrid model for a range of dimensionless settling velocities $w_s = (0.5, 1.0, 2.0) \times 10^{-2}$, Froude numbers $F = 1.19, 1, 0.72$ and dimensionless source radii $r_i = 1, 2, 3$, leading to variations in the value of A_∞ and we plot the results for the position of the front as a function of time (Fig. 8). In these figures, we only plot the radial position up to times at which the volume fraction, ϕ_N drops to 0.01. There is a wide range of behaviour as anticipated because of the range of parameter values (Fig. 8(a)), but when plotted in terms of the rescaled variables, $\hat{r}$ as a function of $\hat{t}$, the spread of behaviours is much less and the evolution follows a 'master curve' more closely (Fig. 8(b)). At the times illustrated in Fig. 8(b) there is still incomplete collapse of the results under this rescaling. However, in the limit of large time, the rescalings R_∞ and T_∞ exactly capture the dependence of the hybrid model solutions on the dimensionless parameters w_s, A_∞ and F. We demonstrate this by calculating the leading-order terms of the late-time asymptotic solution to the hybrid model. Supposing as before that the hybrid model variables r_N, r_J, h_N and ϕ_N are proportional to a power of time at late times, we find by substituting this power-law ansatz into (51), (52), (54) and (59) that

$$\hat{r} = 2 \cdot (3\hat{t})^{1/3} + \cdots, \qquad \hat{h} = 3\hat{t}/4 + \cdots,$$
$$\hat{\delta} = 2/[3 \cdot (3\hat{t})^{1/3}] + \cdots, \qquad \phi = (16/9)\hat{t}^{-7/3} + \cdots. \quad (61)$$

The absence of any dependence on the dimensionless parameters w_s, A_∞ and F reflects the appropriate choice of rescaled variables (58) for the late time evolution.

Bonnecaze et al. [7] report experimental results of the radial position of a particle-driven gravity current due to a sustained flux within a 'sector' tank. They examined four conditions by varying the source flux, the size of particles and their initial concentration. On the assumption that the sidewalls of the sector tank played a negligible role, they modelled these currents using a radially spreading shallow layer model of the gravity current motion. They demonstrated that reasonably accurate predictions of the experimentally-measured propagation could be obtained by the numerical integration of the governing equations, using a constant Froude number $F = 0.72$ in the condition at the front (9); the
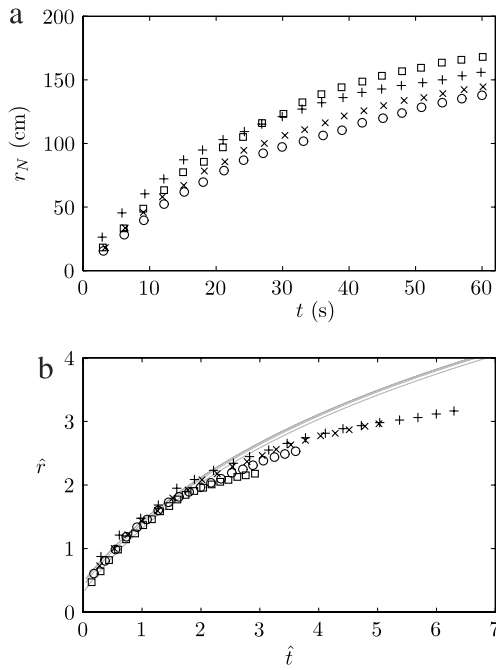
Fig. 9. The experimentally measured front position of a radially spreading particle-driven gravity current as function of time. In (b) the data is plotted in terms of the rescaled variables $\hat{r}$ and $\hat{t}$. The grey curves correspond to numerical results from the hybrid model with parameters corresponding to each of the four experiments, and using the value $F = 0.72$ suggested by [7]. ($\times$: $q = 130$ cm^3 s^{-1}, $g'_0 = 10$ cm s^{-2}, $w_s = 0.36$ cm s^{-1}. +: $q = 130$ cm^3 s^{-1}, $g'_0 = 20$ cm s^{-2}, $w_s = 0.36$ cm s^{-1}. $\square$: $q = 130$ cm^3 s^{-1}, $g'_0 = 10$ cm s^{-2}, $w_s = 0.17$ cm s^{-1}. $\circ$: $q = 75$ cm^3 s^{-1}, $g'_0 = 10$ cms^{-2}, $w_s = 0.17$ cm s^{-1}).
Source: Data from [7].

agreement is quite good only during the initial stages, after which, as the motion slows, viscous forces potentially begin to play a role. These results are plotted in Fig. 9(a), (b). Here we plot the dimensional data and also this data replotted in terms of the re-scaled variables $\hat{r}$ and $\hat{t}$. We note that this rescaling has collapsed the data to a single 'master curve', which is reasonably well fitted by a representative curve from the hybrid model with $F = 0.72$, the value suggested by Bonnecaze et al. [7] for continuously-supplied particle-driven flows.

5. Summary

The hybrid model has been shown to reproduce accurately the motion of sustained, radially spreading, buoyancy-driven flows in scenarios where conventional integral model and naive scaling analyses fail. The new model exploits the structure of the flow, namely a steady-state tail and an unsteady head, to derive a reduced model in terms of just a few coupled ODEs that are simple to solve numerically. Results for compositionally-driven flows follow exactly the same behaviour as that found by numerically integrating the unsteady shallow water equations at long times after release. Moreover the hybrid model captures satisfactorily the initial behaviour and because it introduces no adjustable parameters, it provides a very useful tool for computing the behaviour of a number of environmentally relevant flows, such as the propagation of volcanic ash intrusions.

By 'no adjustable parameters' we mean that the hybrid model uses exactly the same input parameters as the more complex shallow-water model, and no manipulation or addition of parameters was made for achieving the reported agreement between the models. Admittedly, in the problem under investigation F is a semi-empirical, or empirical, value. Our point is that we use an 'off the

shelf' number. The agreement with the shallow-water solution is good when the same F is used in both models.

A clear-cut outcome of our analysis is that in cases of interest (when the radius of propagation is large compared to that of the source) the major part of the influxed volume is in the head domain, not in the steady-state tail. On the other hand, the head plays a minor role in the sedimentation of particles because the fluid that is influxed into the head loses particles along the way; under the assumption of our model that particles are vertically well-mixed within the current, ϕ decays exponentially with r^2 in the tail. These observations may be of importance in the understanding of the spread of volcanic clouds.

Due to its simplicity, the hybrid model can be easily used for the investigation of other effects of interest in the context of volcanic plumes, such as the propagation of the plume after the source is stopped at some t_e (after the eruption ceases), or the influence of different values of r_i, which is determined by conditions at the vent of the volcano and the dynamics of the vertically-rising portion of the plume. On the other hand, we note that numerous practical applications are incompatible with the axisymmetric assumption of the present model, such as the influence of winds on volcanic plumes [23]. A quite complicated modification of the model is needed to relax the assumption of axisymmetry. These topics require additional work and are left for future papers. Additionally, at late times in a volcanic eruption, centrifugal-Coriolis effects due to the rotation of the Earth become important, and an extension of the hybrid model which takes these effects into consideration is under way.

The hybrid model has also been applied to sustained particle-driven flows, demonstrating its success in accurately representing the motion in terms of a simple set of governing ODEs. Here a very considerable advantage is that the model reveals the lengthscales and timescales for the runout of these flows, in terms of the fundamental parameters that characterise the motion. These scales, given in dimensional form by

$$R_\infty = \left(\frac{F^4 A_\infty^3 q^3}{w_s^4 g'} \right)^{1/7} \quad \text{and} \quad T_\infty = \left(\frac{A_\infty^2 q^2}{w_s^5 g'^3 F^2} \right)^{1/7}, \qquad (62)$$

are therefore the analogy for sustained radial currents of 'box' model scalings for instantaneous slumps of suspended particles. They provide important quantitative insights into how the motion is influenced by particle settling that progressively reduces the buoyancy of the current.

Appendix A. The jump conditions at r_J

The speed, height and volume fraction formulae at the jump at r_J are obtained as follows. The dependent variables before the jump are denoted by h_{J-}, u_{J-} and ϕ_{J-} and after the jump are given by h_{J+}, u_{J+} and ϕ_{J+}. In the cases of interest $h_{J+} > h_{J-}$. We use a control volume of height H and with a width much smaller than r_J, allowing curvature terms due to the axisymmetric geometry to be neglected. This control volume moves with the jump at speed $c = \mathrm{d}r_J/\mathrm{d}t$ in positive r direction, and we denote the radial velocity in this frame of reference by $u' = u - c$.

In this moving frame of reference, we impose continuity of fluid and particle volume flux and balance the inviscid momentum flux.

$$q_J = u'_{J-} h_{J-} = u'_{J+} h_{J+}, \tag{A.1}$$

$$q_J \phi_{J-} = q_J \phi_{J+}, \tag{A.2}$$

$$q(\rho_{cJ+} u'_{J+} - \rho_{cJ-} u'_{J-}) = F_J; \tag{A.3}$$

where

$$F_J = \int_0^H p_{J-}(z) \, dz - \int_0^H p_{J+}(z) \, dz \tag{A.4}$$

is the net pressure force, and ρ_c is the density of the current. The height H must encompass the current. We assume that $h_{J+} > h_{J-}$ and hence $H = h_{J+}$ can be taken.

Combining (A.1) and (A.3), we can write

$$(u'_{J-})^2 \frac{h_{J-}}{h_{J+}} (h_{J-} - h_{J+}) = F_J / \rho. \tag{A.5}$$

Recalling that $u'_{J-} = u_{J-} - U$, we note that $U < u_{J-}$, to ensure that energy is dissipated rather than created at the jump [25]. The relevant jump speed result is therefore

$$U = u_{J-} - \left[\frac{h_{J+}}{h_{J-}} \frac{1}{h_{J-} - h_{J+}} (F_J / \rho) \right]^{1/2}. \tag{A.6}$$

The calculation of F_J uses the facts: (1) the pressure is hydrostatic on both sides of the jump, in both the current and the ambient fluids; the hydrostatic pressure, on either side of the jump, is continuous at the interface $z = h_i$. In what follows, the subscripts a, c denote the ambient and the current, respectively.

We use the one-layer shallow water pressure calculations (see [14, Section 12.2]). Briefly: the density of the current is the constant ρ_c, and of the ambient $\rho_c + \lambda z$, where $\lambda = d\rho_a / dz = $ constant (negative). We employ the hydrostatic equation and continuity of pressure at the interface, and obtain:

$$p_a = -\rho_0 gz - \frac{1}{2} \lambda g z^2;$$

$$p_{cJ\pm} = (\rho_c - \rho_0) g h_{J\pm} - \rho_c g z - \frac{1}{2} \lambda g h_{J\pm}^2. \tag{A.7}$$

In the calculation of F_J over $z \in [0, h_{J+}]$ the integral on the $r = r_{J-}$ side is performed on both p_{cJ-} (over $[0, h_{J-}]$) and p_a (over $[h_{J-}, h_{J+}]$); on the $r = r_{J+}$ side, the integration is performed only over p_{cJ+} (over $[0, h_{J+}]$). The result is

$$F_J / \rho_0 = \frac{g}{2} \frac{\rho_c - \rho_0}{\rho_0} \left(h_{J-}^2 - h_{J+}^2 \right) + \frac{1}{3} \left[\frac{-\lambda g}{\rho_c} \right] \left(h_{J-}^3 - h_{J+}^3 \right) \tag{A.8}$$

$$= \frac{g'}{2} \left(h_{J-}^2 - h_{J+}^2 \right) + \frac{\mathcal{N}^2}{3} \left(h_{J-}^3 - h_{J+}^3 \right). \tag{A.9}$$

Substitution into (A.5) and adopting dimensionless hybrid model variables yields, after some algebra, (19) and (33).

Appendix B. The steady inviscid tail of particle-driven gravity currents

For sustained flows through a uniform environment due to a density difference associated only with the presence of suspended relatively dense particles, the dimensionless governing equations are

$$ruh = 1, \tag{B.1}$$

$$\phi = \exp\left(-\frac{w_s(r^2 - r_i^2)}{2} \right) \tag{B.2}$$

and

$$\frac{1}{r} \frac{d}{dr} (ru^2 h) + \frac{1}{2} \frac{d}{dr} (\phi h^2) = 0. \tag{B.3}$$

In this appendix, we examine the far-field form of such flows, based on the assumption that the dimensionless settling velocity is small ($w_s \ll 1$). This introduces a long radial lengthscale of order $w_s^{-1/2} \gg r_i$, over which significant settling occurs, while the flow speed and depth adjust to the local pressure gradients over much shorter radial distances. We employ the method of multiple scales to deduce the form of these fields. Thus we treat the height and velocity as functions of both r and $R = w_s^{1/2} r$, while the volume fraction is given by

$$\phi = \exp(-R^2/2). \tag{B.4}$$

Embedding this into the governing equation gives

$$\left(\frac{\partial}{\partial r} + w_s^{1/2} \frac{\partial}{\partial R} \right) (u^2 + 2\phi h) = -w_s^{1/2} \phi R h, \tag{B.5}$$

subject to $u^2 + 2\phi h = A_0^2$ at $r = r_i$. Seeking solutions of the form $u = u_0 + w_s^{1/2} u_1 + \cdots$ and $h = h_0 + w_s^{1/2} h_1 + \cdots$, we find that at leading order

$$u_0^2 + 2\phi h_0 = A^2(R), \tag{B.6}$$

where $A(R)$ is determined by expanding to $O(w_s^{1/2})$ and applying a consistency condition to keep u_1 smaller than u_0 in the far-field. This demands

$$\frac{\partial}{\partial R} (A^2) = -\exp(-R^2/2)Rh. \tag{B.7}$$

In the far field ($r \gg 1$), we find that $u = A + \cdots$ and $h = 1/(Ar) + \cdots$. Thus we find that

$$\frac{\partial}{\partial R} (A^2) = -\frac{w_s^{1/2} \exp(-R^2/2)}{A}, \tag{B.8}$$

and this may be integrated to give

$$A(R)^3 = A_0^3 - w_s^{1/2} \frac{3}{2} \int_0^R \exp(-s^2/2) \, ds. \tag{B.9}$$

This result is used in the long time reduction of the hybrid model for particle-driven gravity currents. Recalling that $w_s \ll 1$, we may therefore evaluate the leading order expression for the velocity in the far-field

$$A \to A_0 - w_s^{1/2} \frac{\sqrt{\pi}}{2\sqrt{2}} \quad \text{as } R \to \infty. \tag{B.10}$$

References

[1] R. Garvine, Radial spreading of buoyant, surface plumes in coastal waters, J. Geophys. Res. 89 (C2) (1984) 1989–1996.

[2] C. Lemckert, J. Imberger, Axisymmetric intrusive gravity currents in linearly stratified fluids, J. Hydraul. Eng. ASCE 119 (1993) 662–679.

[3] A. Woods, J. Kienle, The dynamics and thermodynamics of volcanic clouds: theory and observations from the April 15 and April 21, 1990 eruptions of Redoubt Volcano, Alaska, J. Volcanol. Geotherm. Res. 62 (1) (1994) 273–299.

[4] C. Johnson, A. Hogg, H. Huppert, R. Sparks, J. Phillips, A. Slim, M. Woodhouse, Modelling intrusions, J. Fluid Mech. (2014) submitted for publication.

[5] M. Woodhouse, A. Hogg, J. Phillips, R. Sparks, Interactions between volcanic plumes and wind during the 2010 Eyjafjallajökull eruption, Iceland, J. Geophys. Res. 118 (2013) 92–109.

[6] C. Spinetti, S. Barsotti, A. Neri, M.F. Buongiorno, F. Doumaz, L. Nannipieri, Investigation of the complex dynamics and structure of the 2010 Eyjafjalla-jökull volcanic ash cloud using multispectral images and numerical simulations, J. Geophys. Res. 118 (10) (2013) 4729–4747. http://dx.doi.org/10.1002/jgrd.50328.

[7] R. Bonnecaze, M. Hallworth, H. Huppert, J. Lister, Axisymmetric particle-driven gravity currents, J. Fluid Mech. 294 (1995) 93–122.

[8] M. La Rocca, C. Adduce, P. Mele, G. Sciortino, Numerical simulation of 3D submarine turbidity currents, in: Proc. 19th International Offshore and Polar Engineering Conference (Osaka, Japan, June 2009), The International Society of Offshore and Polar Engineers (ISOPE), 2009.

[9] E. Meiburg, B. Kneller, Turbidity currents and their deposits, Annu. Rev. Fluid Mech. 42 (2010) 135–156.

[10] D. Hoult, Oil spreading on the sea, Annu. Rev. Fluid Mech. 4 (1972) 341–368.

[11] H. Huppert, J. Simpson, The slumping of gravity currents, J. Fluid Mech. 99 (1980) 785–799.

[12] M. Ungarish, H. Huppert, On gravity currents propagating at the base of a stratified ambient, J. Fluid Mech. 458 (2002) 283–301.

[13] M. Ungarish, Intrusive gravity currents in a stratified ambient: shallow-water theory and numerical results, J. Fluid Mech. 535 (2005) 287–323.

[14] M. Ungarish, An Introduction to Gravity Currents and Intrusions, Chapman and Hall/CRC, 2009.

[15] T. Benjamin, Gravity currents and related phenomena, J. Fluid Mech. 31 (1968) 209–248.

[16] A. Hogg, M. Ungarish, H. Huppert, Particle-driven gravity currents: asymptotic and box-model solutions, Eur. J. Mech. B/Fluids 338 (2000) 139–165.

[17] A. Hogg, M. Ungarish, H. Huppert, Effects of particle sedimentation and rotation on axisymmetric gravity currents, Phys. Fluids 13 (2001) 3687–3698.

[18] J.-C. Chen, Studies on gravitational spreading currents (Ph.D. thesis), California Institute of Technology, 1980.

[19] R. Sparks, M. Bursik, S. Carey, J. Gilbert, L. Glaze, H. Sigurdsson, A. Woods, Volcanic Plumes, John Wiley & Sons, 1997.

[20] A. Slim, H. Huppert, Axisymmetric, constantly supplied gravity currents at high Reynolds number, J. Fluid Mech. 675 (1) (2011) 540–551.

[21] T. Richards, Q. Aubourg, B. Sutherland, Radial intrusions from turbulent plumes in uniform stratification, Phys. Fluids 26 (2014) 036602.

[22] T. Zemach, Simulation of non-homogeneous flow fields subject to rotation and gravity effects (Ph.D. thesis), Technion, Haifa, Israel, 2007.

[23] P. Baines, The dynamics of intrusions into a density-stratified crossflow, Phys. Fluids 25 (2013) 076601.

[24] M. Bursik, R. Sparks, J. Gilbert, S. Carey, Sedimentation of tephra by volcanic plumes: I. theory and its comparison with a study of the Fogo A plinian deposit, Sao Miguel (Azores), Bull. Volcanol. 54 (4) (1992) 329–344.

[25] G. Whitham, Linear and Nonlinear Waves, John Wiley & Sons. Inc., 1974.